International Journal of Applied Earth Observation and Geoinformation 23 (2013) 155–164

Contents lists available at SciVerse ScienceDirect

International Journal of Applied Earth Observation and Geoinformation

journal homepage: www.elsevier.com/locate/jag

Estimating very high resolution urban surface temperature using a spectral unmixing and thermal mixing approach

Chengbin Deng, Changshan Wu*

Department of Geography, University of Wisconsin-Milwaukee, P.O. Box 413, Milwaukee, WI 53201, USA

ARTICLE INFO

Article history:
Received 16 September 2012
Accepted 10 January 2013

Keywords:
Land surface temperature
Impervious surface fraction
Spectral unmixing
Thermal mixing

ABSTRACT

Land surface temperature (LST) plays a critical role in characterizing energy exchanges of the Earth's surface and atmosphere. Recent advances in thermal infrared (TIR) remote sensing technology enable the emergence of airborne very-high-resolution (VHR) TIR sensors to identify detailed LST distribution for environmental, geological and urban applications. However, the usage of airborne VHR TIR data may be limited by its high cost, long acquisition period, extensive data processing, etc. A cost-effective alternative could be VHR LST estimation. We proposed a physically based method, referred to as the VHR spectral unmixing and thermal mixing (VHR-SUTM) approach, to estimate LST at the meter level. Particularly, considering both spectral and thermal properties, spectral unmixing was employed to estimate fractional urban compositions for a comprehensive representation of heterogeneous urban surfaces. Further, VHR LST was modeled as a summation of the thermal features of representative urban compositions weighted by their respective abundances. Results suggest a high agreement between the resampled VHR LST estimates and the retrieved LSTs. With relatively high estimation accuracy (RMSE of 2.02 K and MAE of 1.51 K), the VHR-SUTM technique could serve as a promising and practical method for various applications in urban and environment studies.

© 2013 Elsevier B.V. All rights reserved.

1. Introduction

As an important environmental factor, land surface temperature (LST) plays a critical role in characterizing energy exchanges of the Earth's surface and atmosphere (Quattrochi and Luvall, 1999; Weng, 2009). A prominent example is the surface urban heat island (SUHI) phenomenon, which suggests that LST over an urban area is generally higher than that in its neighboring non-urbanized areas. With natural vegetated lands replaced by a wide range of anthropogenic materials during the process of urbanization, most physical properties of land surface, including albedo, heat capacity, conductivity, moisture, emissivity, etc., have been considerably modified, and accordingly resulted in decreased evapotranspiration (Shoshany et al., 1994; Friedl, 2002; Streutker, 2002; Chudnovsky et al., 2004). From a remote sensing perspective, such an urban–rural surface temperature variation can be detected using appropriate thermal sensors. Thermal infrared (TIR) remote sensing images, ranging from coarse resolution (e.g. Advanced Very High Resolution Radiometer (AVHRR) and Moderate Resolution Imaging Spectroradiometer (MODIS)) to medium resolution (e.g. Landsat Thematic Mapper (TM) and Enhanced Thematic Mapper Plus (ETM+), and Advanced Spaceborne Thermal Emission and Reflection Radiometer (ASTER)), have been widely employed for analyzing urban climate and environments (Streutker, 2003; Nichol, 1994, 2005; Lu and Weng, 2006; Weng, 2009). Moreover, the U.S. National Research Council (NRC) recently reported the Hyperspectral Infrared Imager (HyspIRI) decadal survey mission (NRC, 2007), according to which new spaceborne sensors with visible, near-infrared, shortwave infrared, and TIR wavebands will be launched. The potential TIR imagery of HyspIRI at a spatial resolution of 60 m may substantially improve the ability of thermal information measurement, primarily for the analyses of carbon cycle and ecosystems (Roberts et al., 2012).

In addition to coarse- and medium-resolution TIR imagery, recent advances in TIR technology enable the emergence of airborne very-high-resolution (VHR) thermal sensors to identify detailed LST distribution for a variety of applications, e.g. urban thermal pattern assessment, oil-spill detection, building heat loss mapping, urban energy efficiency monitoring and assessment, geologic mapping, anthropogenic material detection, etc. (Lo et al., 1997; Quattrochi et al., 1998, 2000; Gluch et al., 2006; Hay et al., 2011). In particular, Quattrochi and Ridd (1994, 1998) summarized three merits of VHR TIR imagery for urban thermal pattern analysis, including (1) convenient separation/identification of thermal behaviors of different urban surface materials, (2) spatial aggregation of segments with similarly thermal functions, and (3) inherent integration with various ecological models. In spite of these

* Corresponding author. Tel.: +1 414 229 4860; fax: +1 414 229 3981.
E-mail addresses: cdeng@uwm.edu (C. Deng), cswu@uwm.edu, wuchangshan@gmail.com (C. Wu).

0303-2434/$ – see front matter © 2013 Elsevier B.V. All rights reserved.
http://dx.doi.org/10.1016/j.jag.2013.01.001

advantages, the applications of emerging airborne VHR TIR data are impeded by its limitations, including relatively high cost, long acquisition period, large masses of data, multiple pre-processing steps, etc. (Hay et al., 2011). Consequently, the estimation of VHR LST information could serve as a cost-effective alternative means. A straightforward method is to establish statistical associations between LST and parameters extracted from remote sensing imagery (Voogt and Oke, 2003; Weng, 2009). LST has been estimated through employing a great number of environmental and socio-economic factors, including geometry of street canyon, land use and land cover (LULC) type and change, normalized difference vegetation index (NDVI), green vegetation abundance, impervious surface abundance, landscape metrics, intensity of human activity, population density and distribution, etc. (Eliasson, 1996; Elvidge et al., 1997; Bottyán and Unger, 2003; Yuan and Bauer, 2007; Weng et al., 2011; Li et al., 2011). With current charge-coupled device (CCD) technology, however, only coarse-/medium-resolution TIR imagery can be acquired from spaceborne sensors. Due to the lacks of VHR TIR bands and/or synchronizing field measurements as the dependent variable in simple correlation/regression analysis against environmental indicators, it is impractical to establish such statistical relationships for VHR LST estimation.

One potential solution could resort to the physical mechanism underlying the SUHI phenomenon, particularly the interactions between land surface properties and thermal responses. In addition to the aforementioned statistical analysis, a few studies explored individual thermal responses of various urban land use/cover types using medium- to high-spatial resolution TIR imagery. For instance, Goward (1981) summarized three classes of urban land use types with significantly different thermal properties, i.e. natural areas, pavements, and buildings. Quattrochi and Ridd (1994, 1998) further expanded these three classes into seven more detailed land use types of urban thermal objects. Moreover, in conjunction with Ridd's vegetation–impervious surface–soil (V–I–S) model (Ridd, 1995), diverse diurnal thermal behaviors of a series of urban materials have been examined (Chudnovsky et al., 2004; Hartz et al., 2006; Gluch et al., 2006). Although different separation/classification schemes have been proposed to identify individual urban surface materials with "unique reactions of energy and moisture within an urban ecosystem" (Gluch et al., 2006), rare research has been conducted to model the composite thermal response from individual land covers. Therefore, the overall objective of this paper is to estimate high-resolution urban land surface temperature through incorporating thermal responses from representative urban materials with their respective fractional abundances. To reach this goal, we developed a two-step physically based method, referred to as the VHR spectral unmixing and thermal mixing (VHR-SUTM) approach. More specifically, two explicit objectives of this study are: (1) adopting spectral unmixing to derive fractional urban compositions, with a focus on their thermal responses, and (2) developing thermal mixing to estimate VHR LST through integrating the thermal responses of urban compositions and their respective abundances.

The remainder of this paper is structured as follows. Section 2 introduces study area and data. Section 3 presents the proposed VHR-SUTM method for LST modeling with IKONOS imagery. Modeling results and accuracy assessment are provided in Section 4. Finally, discussion and conclusions are given in Sections 5 and 6, respectively.

2. Study area and data

2.1. Study area

The study area includes the Town and Village of Grafton in Ozaukee County, Wisconsin, USA (see Fig. 1). The western side of the study area is the Town of Grafton, where major land use types include commercial, industrial, high- and medium-density residential, and civic (educational institutes, hospital, and government services) lands (Southeastern Wisconsin Regional Planning Commission (SEWRPC), 2000). The eastern side locates the Village of Grafton by the Lake Michigan, and its dominant land uses are low-density residential, agricultural, forest, wetlands, and other natural lands. The population of Grafton was 14,444 and the number of housing units was 5773 according to 2000 Census, with a growth rate of approximately 8% and 19% from 1990 respectively. Based on predictions from SEWRPC (2004a,b), such a trend of continuous development in Grafton is expected in the coming several decades. Due to the impact of urban LST on environmental health, internal microclimatology, human comfort and energy consumption, detailed urban thermal information may be of great help for planning practices, environmental monitoring and disease prevention and control in the study area. To construct the thermal mixing model, the retrieved LST of Cedarburg (see Fig. 1), an adjacent city of Grafton with almost identical climatic, environmental and socioeconomic status, was adopted to independently derive typical LST values of each land cover composition.

2.2. Dataset and LST retrieval

An IKONOS image acquired on September 3, 2002 with a resolution of 4 m was collected to derive subpixel land cover information. This image was rectified to a Universal Transverse Mercator (UTM) projection with WGS84 datum and UTM zone 16. At-satellite reflectance of this image was then derived from digital numbers (DNs), following the work of Taylor (2009). In addition, to obtain LSTs for model construction and validation, a Landsat TM TIR image acquired on September 6, 2002 was adopted at a resampled 30-m spatial resolution (U.S. Geological Survey, 2010). In addition, an aerial Digital Orthophoto Quarter Quadrangle (DOQQ) image acquired in 2002 was obtained for land cover fraction validation. The datum and projection of these images were set identically as those of the IKONOS image. Because of the cloud-free atmospheric condition and the small geographical extent of the study area, we did not carry out any atmospheric correction for both images. We also collected meteorological data from the University of Wisconsin-Milwaukee field station and the zenith wet delay estimate data (DeMets, 2012) for deriving LST information, respectively.

For LST retrieval from the Landsat TM TIR image, we employed the mono-window algorithm (MWA) proposed by Qin et al. (2001), which takes into account the effects of emissivity and atmosphere. Four important parameters of the MWA model, i.e. emissivity (ε_6), effective mean atmospheric temperature (T_a), brightness temperature (T_6) and atmospheric transmittance (τ_6), were predetermined respectively according to specific land surface properties and atmospheric condition of the study area (Qin et al., 2001; Okwen et al., 2011). First, ε_6 was determined using the NDVI thresholds method developed by Sobrino et al. (2001). Second, T_a was derived based on the acquisition date of the remote sensing image and the geographical location of our study area. Third, T_6 was derived following the work of Markham and Barker (1986) and Landsat 7 science data users handbook (Irish, 2000). Finally, we calculated τ_6 using the linear regression model with the empirical relationship between atmospheric transmittance and water vapor content according to the GPS meteorology method (Qin et al., 2001; Bevis et al., 1992, 1994; Rocken et al., 1995). These four resulting parameters were then input into the MWA model to retrieve LST information. More details of LST retrieval can be referred to Qin et al. (2001) and Okwen et al. (2011).

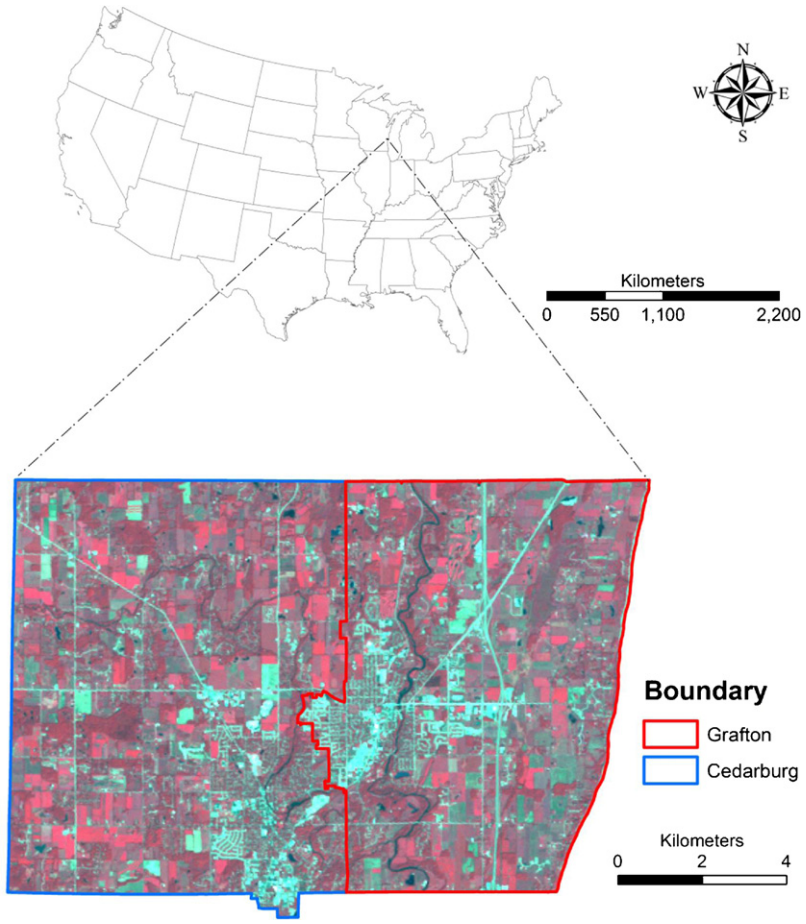

Fig. 1. Study area, Cedarburg and Grafton, Wisconsin, USA, illustrated by a Landsat TM false-color composite image.

3. Methodology

The VHR-SUTM method includes two major steps. First, spectral unmixing was adopted to derive fractional land covers with unique thermal responses. Especially, pure land covers (endmembers) were selected by considering their respective spectral and thermal properties. Moreover, the shadowing problem associated with the VHR imagery was mitigated through adding NDVI as an ancillary band for spectral unmixing. Second, thermal mixing was performed to model per-pixel VHR LST value as a summation of representative LST values weighted by their corresponding land cover fractions. To demonstrate the modeling and validation process of the VHR-SUTM model, a flowchart is illustrated in Fig. 2.

3.1. Spectral unmixing

3.1.1. Endmember selection based on spectral and thermal properties

To derive accurate fractional land covers, we selected representative endmembers that possess unique thermal responses. Different from most traditional spectral mixture analysis (SMA) methods that ignored thermal properties for endmember selections, we chose endmembers through considering both thermal and spectral properties. With general guides in previous UHI/SUHI studies (Goward, 1981; Quattrochi and Ridd, 1994, 1998; Jensen, 2000; Chudnovsky et al., 2004; Hartz et al., 2006; Gluch et al., 2006; Deng and Wu, 2013), we chose five categories of land cover compositions, including vegetation, dark impervious surfaces, bright impervious surfaces, moist soil, and dry soil, to account for the thermal variations of urban land covers. In addition to the thermal response of each endmember, collinearity/multicollinearity among endmember spectra was also carefully considered (Van der Meer and Jia, 2012). Among these five materials, dry bare soil and bright impervious surface share very similar spectral signatures and thermal properties (Jensen, 2000; Gluch et al., 2006). Consequently, these two categories of land cover compositions were grouped into a class of "high-albedo materials". Besides, moist soil and dark impervious surfaces possess similar spectral signatures, but with significantly different thermal properties (Jensen, 2000; Gluch et al., 2006; Small, 2001; Wu and Murray, 2003; Lu and Weng, 2004, 2006). To solve this problem, these two materials were first aggregated into a class of "low-albedo materials" for spectral unmixing, and then separated from each other using an ancillary mask. The generation of this mask will be detailed later. Therefore, a vegetation–high albedo–low albedo (V–H–L) model was first utilized for SMA, then by considering the variations of thermal responses, the Ridd's three-endmember V–I–S were extended to a four-endmember model for VHR LST estimation, i.e. the vegetation–high albedo–dark impervious surface–moist soil (V–H–D–M) model for further thermal mixing.

3.1.2. Shadowing effect mitigation using NDVI

As a long-existing issue with VHR remote sensing imagery (Dare, 2005; Li et al., 2005; Lu, 2007; Wu, 2009; Lu et al., 2010, 2011), the shadowing effect is significant in the study area: the increased spatial resolution in VHR imagery results in spectral confusion between shade/shadow and low-albedo materials. Despite with similar spectra, shadows and low-albedo materials are with significantly different thermal properties, and their confusion could result in inaccurate LST estimations. In order to reduce the impact

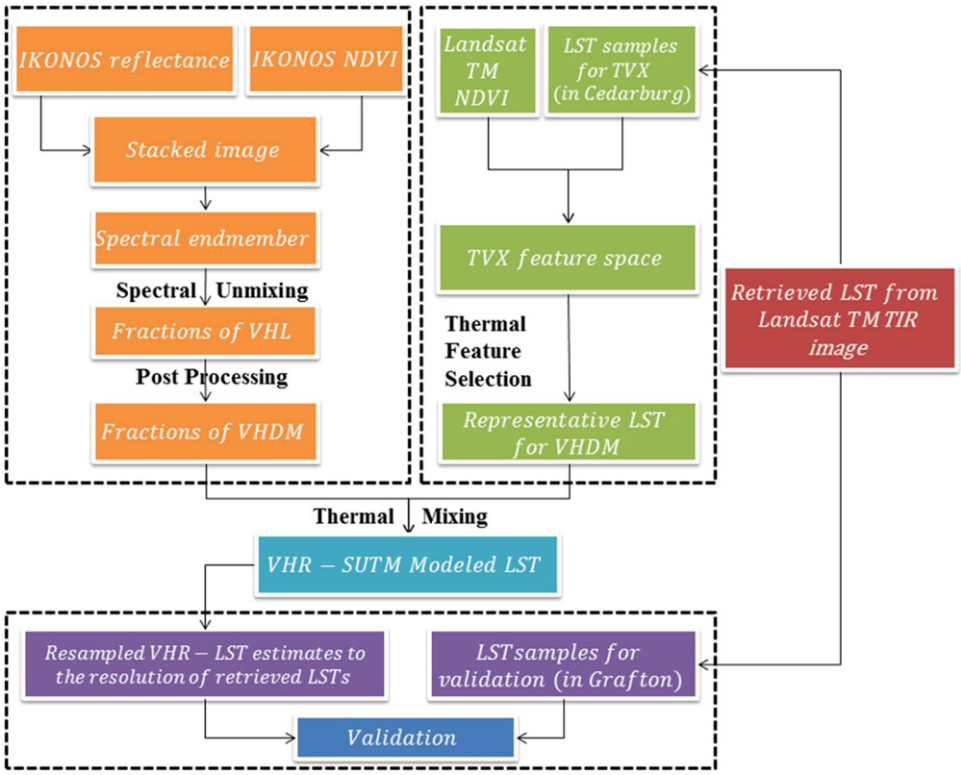

Fig. 2. A flowchart of the VHR-SUTM model.

from shadow and shaded areas on fractional land covers, particularly for the cast shadows in vegetated areas, we adopted NDVI as an additional band for spectral unmixing. We expected that the addition of NDVI could help on identification of vegetation shadows, and therefore the confusion between cast shadow and dark impervious surface can be somewhat alleviated.

3.1.3. Fully constrained SMA

After determining endmembers and including NDVI as an ancillary band of the IKONOS reflectance imagery, we employed a fully constrained SMA for estimating fractional land covers. Under the assumption of spectral signal combination, SMA decomposes per-pixel spectral response into spectra of various homogeneous land cover components weighted by corresponding areal coverage (Smith et al., 1990; Adams et al., 1986, 1995; Roberts et al., 1998), which can be expressed as follows:

$$S_b = \sum_{i=1}^{N} f_i \cdot S_{i,b} + e_b \quad (1)$$

subject to

$$\sum_{i=1}^{N} f_i = 1 \text{ and } f_i \geq 0 \quad (2)$$

where S_b is the spectrum of band b, including all four IKONOS reflectance bands and the NDVI band; N is the number of endmembers; f_i is the resultant fraction of each endmember i; $S_{i,b}$ is the spectra of endmember i in band b; and e_b is the model residual in band b. In this study, endmember fractions were derived through the inverse least squares deconvolution model (Van der Meer and De Jong, 2000; Wu and Murray, 2003).

Subsequently, a mask was adopted to divide the resulting fractional low-albedo material into moist soil and dark impervious surfaces. This mask was derived through post-processing a fractional impervious surface map produced by Wu (2009). Specifically, a simple thresholding method was applied to classify the subpixel impervious surface map into two classes, developed and non-developed lands. Further post-processing steps were carried out to reduce the "pepper and salt" noise in the binary classification map, including: (1) defining the minimum size of contiguous groups of impervious surface pixels empirically, and (2) removing pixel groups with a size smaller than the specified value. With this ancillary mask, the fractional low-albedo material was then separated based on a simple rule: low-albedo materials in non-developed lands were considered as moist soil, while those in developed lands were regarded as dark impervious surface.

3.2. Thermal mixing

After deriving land cover abundances, VHR LST can be modeled as a summation of their representative thermal responses weighted by their respective fractions through a thermal mixing model (Friedl and Davis, 1994; McCabe et al., 2008).

$$T_s = f_v T_v + f_h T_h + f_d T_d + f_m T_m + e \quad (3)$$

subject to

$$f_v + f_h + f_d + f_m = 1 \text{ and } f_v, f_h, f_d, f_m \geq 0 \quad (4)$$

where T_s is the LST estimate of an IKONOS pixel; f_v, f_h, f_d and f_m are fractions of vegetation, high albedo materials, dark impervious surfaces and moist soil, respectively, obtained through spectral unmixing detailed in the previous subsection; T_v, T_h, T_d and T_m are the representative thermal responses of vegetation, high albedo materials, dark impervious surfaces, and moist soil, respectively; e is the model residual.

For calculating representative thermal response of each land cover composition, the Landsat TM image of Cedarburg, WI was employed. The Landsat NDVI was plotted against the retrieved LSTs to derive the temperature-vegetation index (TVX) feature space.

With the TVX triangle, pure land covers were identified through a visual comparison with the Landsat multispectral imagery, and the representative thermal response of each land cover composition was calculated as the mean LST values of the extreme pixels at the vertices or boundaries. The usage of the cross-scale LSTs is under the assumption that, the thermal responses of urban surface materials at a finer resolution remain constant as those at a coarser one. In addition, it is worth emphasizing that, for valid and independent estimation and validation, the retrieved LSTs in Cedarburg were adopted for generating the TVX space and deriving representative LSTs of urban surface materials, while those in Grafton were used for validation.

3.3. Accuracy assessment

In this study, the performances of spectral unmixing and thermal mixing were assessed accordingly. First, the accuracy of V–H–L fractions was assessed through manually digitizing 100 random samples on the DOQQs. A sampling size of 20 m × 20 m was employed to reduce the impacts of geometric errors between images (Powell et al., 2007; Wu, 2004, 2009). Moreover, to examine the impact of the addition of NDVI on the fractional land cover estimates, we further compared the spectral unmixing results with and without NDVI. Second, for the assessment of LST estimates by thermal mixing, the original 4-m VHR LST estimates were first resampled to 30 m, then the resampled LST results were compared with the retrieved LST values over the whole Grafton. This aggregation is because of the lacks of IKONOS TIR bands or synchronizing field-gauged LST measurements. The usage of 30-m resolution for the Landsat TM TIR image is because that its original 120-m resolution has been resampled to and delivered at 30 m by U.S. Geological Survey in consistent with Landsat multispectral bands since February, 2010 due to software reason (U.S. Geological Survey, 2010). We do acknowledge that we should use the 120-m Landsat TM TIR image, if available. Estimation accuracy was assessed using both visual comparisons and quantitative accuracy metrics, including the root mean square error (RMSE) and mean absolute error (MAE). The expressions of RMSE and MAE are given in Eqs. (5) and (6), respectively.

$$\mathrm{RMSE} = \sqrt{\frac{1}{N}\sum_{i=1}^{N}(\hat{T}_i - T_i)^2} \tag{5}$$

$$\mathrm{MAE} = \frac{1}{N}\sum_{i=1}^{N}|\hat{T}_i - T_i| \tag{6}$$

where $\hat{T}_i$ is the modeled LST for pixel i; T_i is the reference LST of pixel i retrieved from the Landsat TM TIR image; N is the total number of sample pixels. As measures of precision, both RMSE and MAE can effectively quantify the relative estimation error at the pixel level.

4. Results

4.1. Land cover composition abundance estimates with spectral unmixing

A multispectral image with five bands was created through stacking four IKONOS reflectance bands and NDVI (see Fig. 3). After performing a principal component analysis (PCA) with this image, we generated a feature space scatterplot between PC 1 and PC 2 to facilitate spectral endmember selection (see Fig. 4). Visual interpretations and comparisons were employed to identify target endmembers of VHL on this scatterplot. With endmembers enclosed in circles at the vertices or boundaries of the feature space,

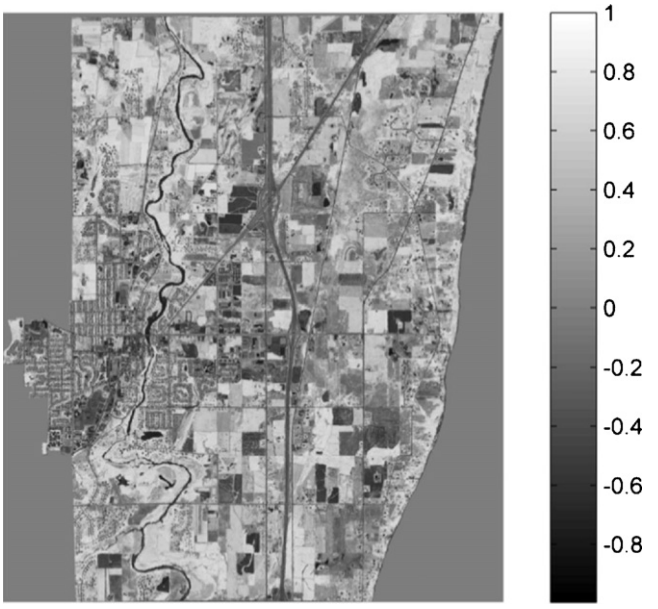

Fig. 3. The resultant IKONOS NDVI.

a fully constrained linear spectral unmixing was then solved to derive individual land cover abundances using Eqs. (1) and (2). The resultant fraction images were illustrated in Fig. 5. It indicates that vegetation (see Fig. 5A) dominates agriculture lands, grasslands and forests in rural areas and parks in urban areas. Comparatively, high albedo materials (see Fig. 5B) are majorly distributed in urban areas, except for a small portion in rural areas. Especially, composed of metal and concrete, etc., bright impervious surfaces are associated with transportation networks and rooftops. In addition, dry bare soil can be found in cultivated agricultural lands in rural areas, particularly in the Village of Grafton. Finally, low albedo materials (see Fig. 5C), including water, moist soil, and dark impervious surfaces, can be observed across the study area. Quantitative accuracy metric suggests adequate unmixing results of these three land cover

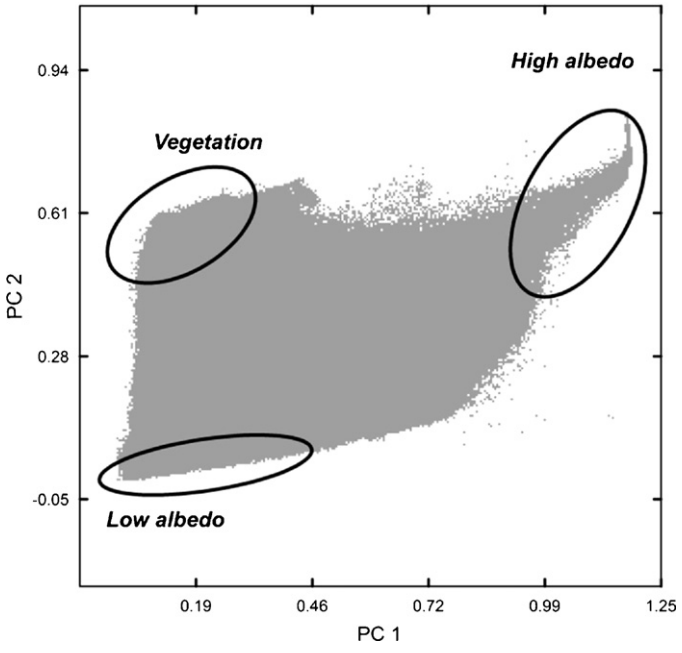

Fig. 4. Endmemer selection in the feature space scatterplot of PCA components generated from the newly stacked VHR image with five bands.

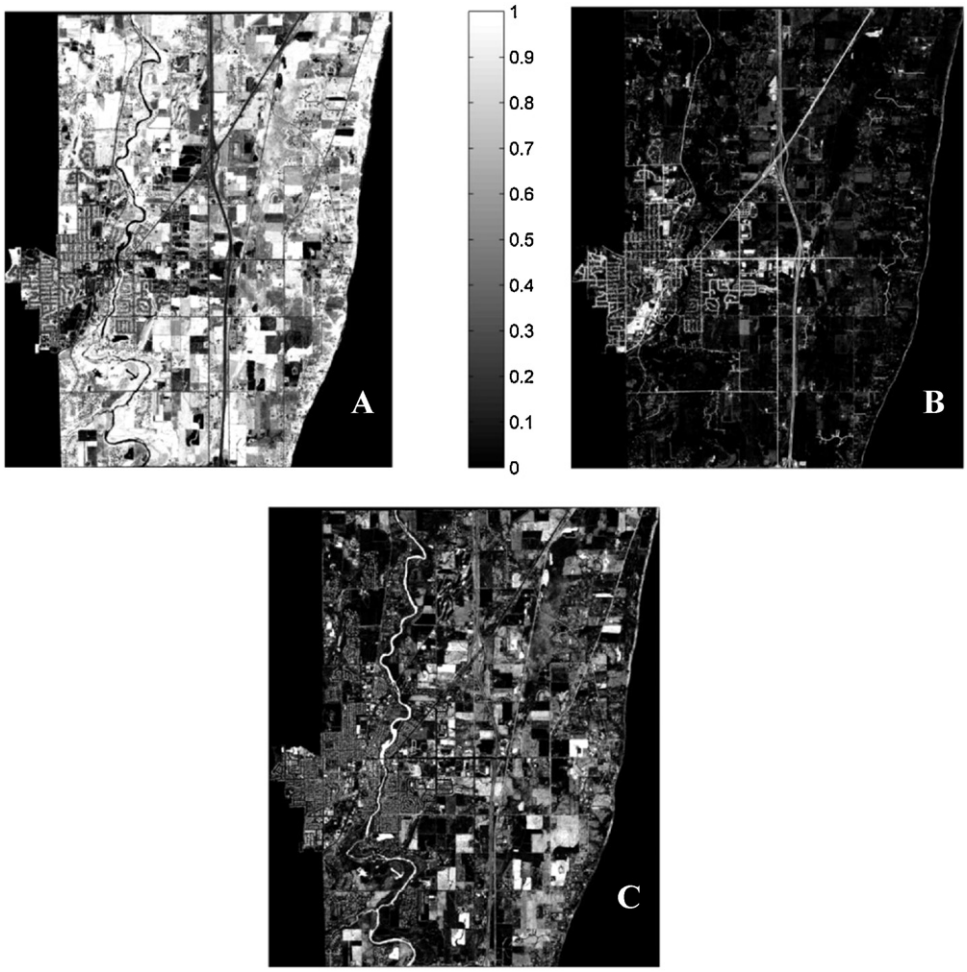

Fig. 5. Resultant fraction images of spectral unmixing: (A) vegetation, (B) high albedo, and (C) low albedo.

fraction estimates, with an MAE of 12.46% for vegetation, 5.24% for high albedo, and 12.45% for low albedo (see Table 1). Moreover, an ancillary mask with binary classes (see Fig. 6) was employed to derive fractions of moist soil and dark impervious surface for thermal mixing.

To illustrate the effectiveness of the stacked image to mitigate the impact of cast shadow, the original IKONOS image was also adopted for SMA for comparison purpose. Fig. 7 demonstrates the resulting land cover fractions of low-albedo materials in a small subset of the study area using both images. As shown in Fig. 7B, without NDVI, the confusion between shade/shadow in forests and dark impervious surfaces is severe, which could further result in significant LST estimation errors if these abundances are applied directly in thermal mixing. On the contrary, it is apparent in Fig. 7C that, with the help of NDVI, the confusions between cast shadow (especially in forests) and other low albedo materials have been significantly removed. Consistent with visual comparisons, a quantitative examination (see Table 1) indicates that, with NDVI, the estimation accuracy improved significantly, with much lower MAEs for vegetation (12.46% vs. 17.32%) and low albedo abundance (12.45% vs. 18.05%). This improvement is probably because, in consistence with the principle of weighted SMA (Somers et al., 2009), the inclusion of NDVI could prioritize certain spectral bands that may maximize the variations among endmembers for SMA.

Table 1
Accuracy of resulting fractional land covers before and after including NDVI as an additional band.

Land cover fraction type	MAE (%) (without NDVI)	MAE (%) (with NDVI)
Vegetation	17.32	12.46
High albedo	4.41	5.24
Low albedo	18.05	12.45

4.2. Thermal feature extraction and LST modeling with thermal mixing

To derive thermal feature of each urban surface composition, we followed previous works for endmember selection on a simplex (Lu and Weng, 2006): extreme pixels with similar thermal response at the vertices of the TVX feature space were selected, and compared visually with their corresponding land cover types in the Landsat image. Through a careful examination, we found that the four target urban surface materials were clustered at various locations of the TVX triangle. The lowest LST values were found at the lower left vertex with low values of both LST and NDVI, representing land covers dominated by wet objects, such as water body and moist soil. The second lowest LST values were associated with vegetation, located at the top vertex of the TVX triangle with the highest NDVI values. On the contrary, pixels with the highest LST were observed at the lower right vertex of the TVX triangle with low NDVI but high LST values, which correspond mainly to dark impervious surfaces. High-albedo materials, including dry bare soil and bright impervious surfaces, were with the second highest LST values, and located on the base boundary of the TVX triangle and next to the cluster of dark impervious surfaces. All four materials were highlighted in

Fig. 6. The ancillary mask for separating dark impervious surface and moist soil.

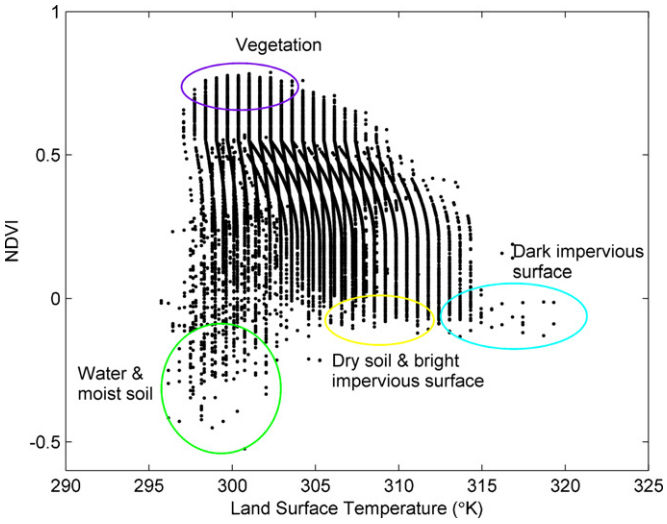

Fig. 8. Thermal feature extraction in a Landsat LST-NDVI (TVX) space.

the TVX triangle in Fig. 8 by circles with various colors, respectively. Accordingly, the representative LST values of each land cover were acquired by averaging these enclosed extreme pixels. Admittedly, due to the similarity to the derivation of spectral endmember signature for SMA, this extraction process of thermal feature on the TVX feature space might be regarded as somewhat subjective (Weng et al., 2008).

With thermal features extracted from the TVX feature space, we assumed that the thermal features of materials in Grafton were the same as those in Cedarburg, as derived and introduced in the

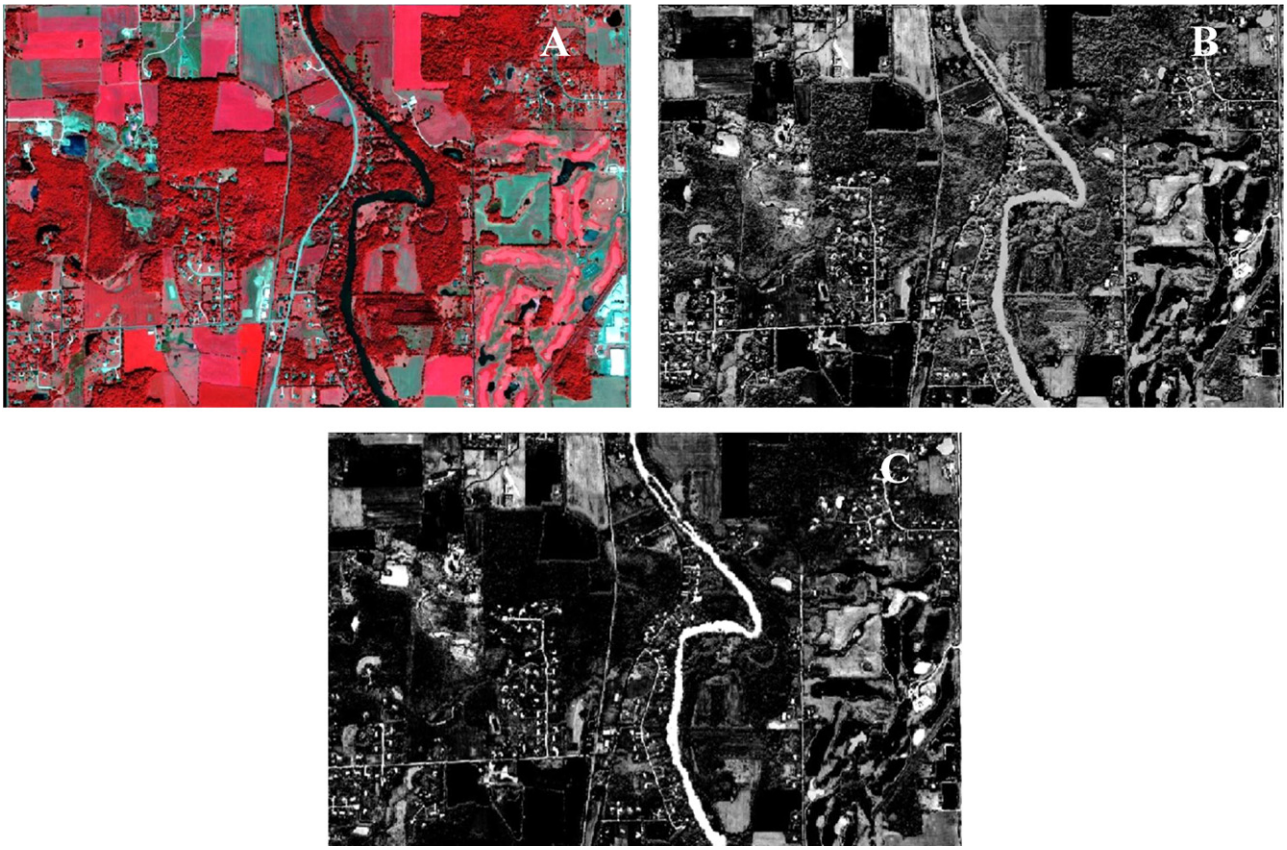

Fig. 7. Comparisons of spectral unmixing results, with (A) a subset of IKONOS false-color composite image, (B) low albedo fraction derived from the original image with four reflectance bands only (without NDVI), and (C) low albedo fraction derived from the stacked image (with NDVI as an additional band).

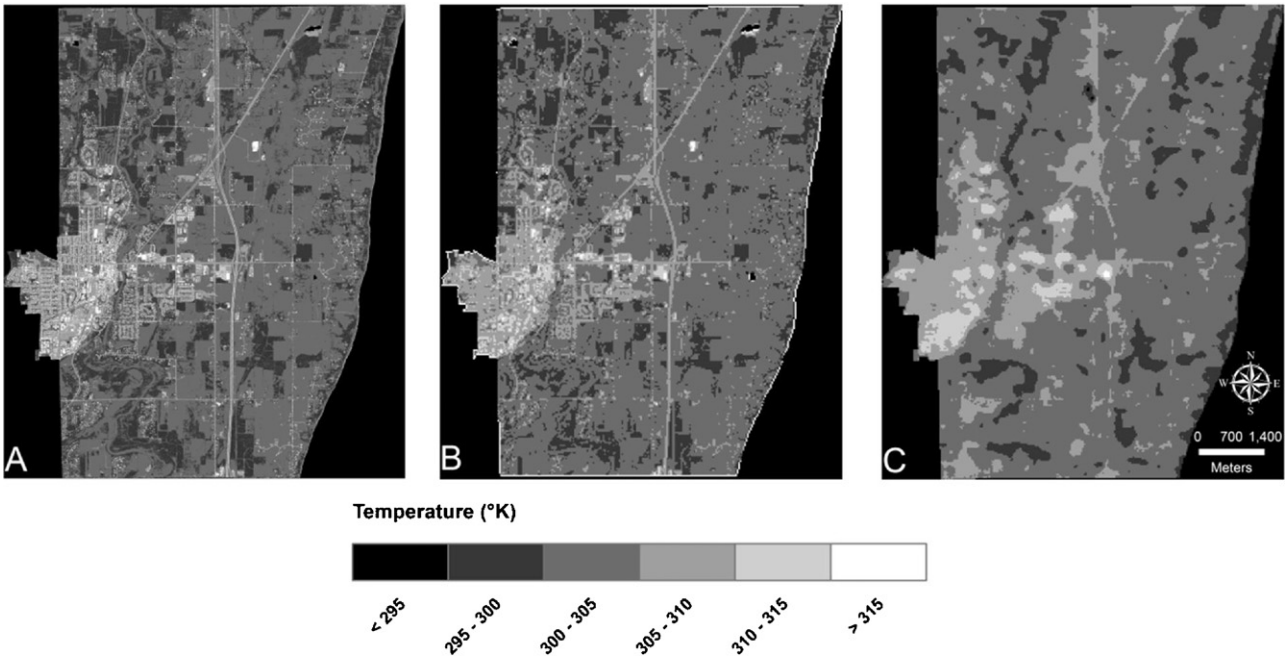

Fig. 9. Comparisons of (A) the original 4-m LST estimates with the VHR-SUTM method, (B) the resampled 30-m LST for comparison purpose, and (C) the retrieved LST from the Landsat TM TIR band.

previous subsection. Therefore, VHR LST of Grafton can be modeled as a composite thermal response of four compositions using Eqs. (3) and (4). Fig. 9A illustrates the LST estimation result at a 4 m resolution. Shown in a white tone, pixels with highest LST estimates were found in areas with dark impervious surfaces, such as asphalt parking lots and roadways in commercial lands. The second highest LST estimates, characterized by light gray tone, were mostly observed in areas with a high percentage of dry bare soil, or bright impervious surfaces. These bright impervious surfaces are composed of concrete, and distributed in transportation networks, sidewalks, driveways, rooftops, etc. Highlighted with a dark gray to black tone, pixels dominated by vegetation and moist soil possess the lowest LST estimates, generally located in the Village of Grafton with various natural lands including forests, grasslands, wetlands, etc. Overall, a general agreement of spatial distribution was found between impervious surfaces and warm materials, as well as between vegetation and moist soil dominated natural lands and cool materials, which is consistent with previous research (Quattrochi and Ridd, 1994, 1998; Chudnovsky et al., 2004; Gluch et al., 2006; Lu and Weng, 2006).

To assess the performance of VHR-SUTM, the retrieved LST map (see Fig. 9C) was adopted for reference LST as an alternative, due to the lack of synchronizing in situ measurements. Then the 4-m VHR LST estimation results (see Fig. 9A) have to be further resampled to the 30-m spatial resolution in conjunction with that of the Landsat TIR image (see Fig. 9B). Visual comparison finds high agreement between the LST estimates and reference values (see Fig. 9B and C respectively). This observation is also supported by two quantitative accuracy metrics: the overall RMSE and MAE are 2.017 K and 1.505 K, respectively. Although relatively high accuracy can be derived with this method, errors are still observed in a few pixels from two potential sources. First, overestimations are found in a small number of pixels that are mistakenly identified as impervious surfaces with higher LST values. These pixels are actually mixtures of materials with lower thermal responses, including metal, water body, etc. Second, underestimations are observed in vegetated areas, particularly in forest lands with trees and shrubs. It might be explained by the thermal instability nature of trees and shrubs with large standard deviation of radiance (Gluch et al., 2006), possibly with pertinence to their various background substrates with different thermal properties (Roberts et al., 2012).

5. Discussion

A significant difficulty in the SUHI research is the lack of a comprehensive characterization of the heterogeneous urban surface, which prevents further explorations of the land–atmosphere interaction (Voogt and Oke, 2003). With a focus on the relationship between thermal response and land cover composition, the VHR-SUTM model attempts to combine approaches of spectral unmixing and thermal mixing to seek a potential solution to this problem: urban surface can be characterized by subpixel urban composition abundance through spectral unmixing; representative thermal properties of these urban compositions can be extracted through analyzing the TVX feature space; and consequently the overall urban thermal pattern can be modeled through the integration of these two factors by thermal mixing.

In the spectral unmixing step, an important consideration is to address the paradox between thermal variation and spectral confusion for endmember selection. On one hand, due to the within-class thermal variation, it is necessary to further partition a general land cover class into several subclasses to characterize their different thermal responses. For example, we initially divided impervious surfaces into dark and bright impervious surfaces, while soil is further divided into dry and moist soil. On the other hand, the increasing number of subclasses, however, could lead to severe spectral confusion between target endmembers, which increases the risk of spectral collinearity in spectral unmixing (Van der Meer and Jia, 2012). To balance the requirements and limitations of both spectral and thermal properties, three processing steps were developed. First, due to the spectral and thermal similarity, bright impervious surfaces and dry soil were aggregated into a group of high-albedo materials. Second, considering spectral collinearity and between-class thermal variation, dark impervious surfaces and moist soil were first aggregated as a group of low-albedo material for SMA, and then were separated with the help of an ancillary mask. Third, to remove the shadowing effect, we stacked NDVI as

an additional band into the original IKONOS multispectral image to include more terrestrial information for spectral unmixing. Taking into consideration both spectral and thermal responses of urban surface compositions, we extended Ridd's V–I–S model into a four-endmember V–H–D–M model in SMA for urban thermal pattern analysis.

In spite of the merits in this pilot study, a major limitation in this study is the lack of ground VHR LST observations for validation, and admittedly, it was difficult to validate the LST estimates at the 4-m resolution through the proposed VHR-SUTM method. As an alternative at current stage, we had to resample the 4-m LST estimates to a coarser resolution of 30 m in consistence with those of Landsat TIR image acquired from U.S. Geological Survey. Although high agreement was achieved for the resampled LST estimates, further research with synchronizing field measurements is necessary to perform a more comprehensive validation.

6. Conclusions

VHR LST information is an essential factor in environmental, geological and urban applications. Due to the limitations of airborne VHR TIR remote sensing imagery, the estimation of LST information may be a cost-effective alternative. To reach this goal, a potential mechanism for understanding detailed urban thermal pattern has been proposed in this study. Specifically, to assist in exploring the interplay between high resolution land cover composition and detailed urban thermal pattern, we utilized subpixel land cover information in an attempt to provide a comprehensive representation of urban surface. To derive accurate urban composition abundances, we selected endmembers based on both spectral and thermal properties for SMA, with which the paradox between thermal variation and spectral similarity was addressed. With the resulting subpixel urban information, as well as identified cross-scale thermal features, VHR urban thermal distribution was modeled through integrating thermal responses of individual surface materials and their respective abundance.

Two major conclusions can be drawn from the analyses of the VHR LST estimation process. First, by considering the requirements and limitations of both spectral and thermal properties, spectral confusions of three low-albedo objects (i.e. shade/shadow, moist soil and dark impervious surface) were mitigated, and their impact on the fractional land cover estimation accuracy was reduced. Particularly, impacts from cast shadows were reduced by employing NDVI as an additional band for spectral unmixing. Besides, moist soil and dark impervious surface were grouped as a "low albedo" category for SMA, and further separated using an ancillary mask. Second, a high agreement can be found between the VHR-SUTM modeled LSTs and the retrieved LSTs using both visual comparison and quantitative assessment (RMSE of 2.02 K and MAE of 1.51 K). Therefore, the VHR-SUTM technique could serve as a promising and practical method in urban and environmental studies, including characterization of urban/suburban infrastructures, geologic mapping, identification of potential habitats of infectious disease vectors, etc. Admittedly, due to the lack of synchronizing field measurements, more efforts should be put on for a comprehensive validation in future studies.

Acknowledgments

This research was partially supported by UWM Research Growth Initiative (RGI). The authors would like to thank anonymous reviewers for their constructive comments. We are grateful to Prof. Chunk DeMets of the University of Wisconsin-Madison for generously providing the GPS ZWD estimates data.

References

Adams, J.B., Smith, M.O., Johnson, P.E., 1986. Spectral mixture modeling: a new analysis of road and soil types at the Viking Lander site. Journal of Geophysical Research 91, 8098–8112.

Adams, J.B., Sabol, D.E., Kapos, V., Almeida Filho, R., Roberts, D.A., Smith, M.O., 1995. Classification of multispectral images based on fractions of endmembers: application to land-cover change in the Brazilian Amazon. Remote Sensing of Environment 52, 137–154.

Bevis, M., Businger, S., Herring, T.A., Rocken, C., Anthes, R.A., Ware, R.H., 1992. GPS meteorology: remote sensing of atmospheric water vapor using the Global Positioning System. Journal of Geophysical Research 97, 15,787–15,801.

Bevis, M., Chiswell, S., Herring, T.A., Anthes, R.A., Rocken, C., Ware, R.H., 1994. GPS meteorology: mapping zenith wet delays onto precipitable water vapor. Journal of Applied Meteorology 33, 379–386.

Bottyán, Z., Unger, J., 2003. A multiple linear statistical model for estimating the mean maximum urban heat island. Theoretical and Applied Climatology 75 (3–4), 233–243.

Chudnovsky, A., Ben-Dor, E., Saaroni, H., 2004. Diurnal thermal behavior of selected objects using remote sensing measurements. Energy and Buildings 36, 1063–1074.

Dare, P.M., 2005. Shadow analysis in high-resolution satellite imagery of urban areas. Photogrammetric Engineering and Remote Sensing 71 (2), 169–177.

DeMets, C., 2012. Personal communication.

Deng, C., Wu, C., 2013. Examining the impacts of urban biophysical compositions on surface urban heat island: a spectral unmixing and thermal mixing approach. Remote Sensing of Environment 131, 262–274.

Eliasson, I., 1996. Urban nocturnal temperatures, street geometry and land use. Atmospheric Environment 30 (3), 379–392.

Elvidge, C.D., Baugh, K.E., Kihn, E.A., Kroehl, H.W., Davis, E.R., Davis, C.W., 1997. Relation between satellite observed visible-near infrared emissions, population, economic activity and electric power consumption. International Journal of Remote Sensing 18 (6), 1373–1379.

Friedl, M., 2002. Forward and inverse modeling of land surface energy balance using surface temperature measurements. Remote Sensing of Environment 79 (2), 344–354.

Friedl, M.A., Davis, F.W., 1994. Sources of variation in radiometric surface temperature over a tallgrass prairie. Remote Sensing of Environment 48 (1), 1–17.

Gluch, R., Quattrochi, D.A., Luvall, J.C., 2006. A multi-scale approach to urban thermal analysis. Remote Sensing of Environment 104 (2), 123–132.

Goward, S.N., 1981. Thermal behavior of urban landscapes and the urban heat island. Physical Geography 2, 19–33.

Hartz, D.A., Prashad, L., Hedquist, B.C., Golden, J., Brazel, A.J., 2006. Linking satellite images and hand-held infrared thermography to observed neighborhood climate conditions. Remote Sensing of Environment 104, 190–200.

Hay, G.J., Kyle, C.D., Hemachandran, B., Chen, G., Rahman, M., Fung, T.S., Arvai, J.L., 2011. Geospatial technologies to improve urban energy efficiency. Remote Sensing 3, 1380–1405.

Irish, R.R., 2000. Landsat 7 science data users handbook, Report 430-15-01-003-0. National Aeronautics and Space Administration. http://landsathandbook.gsfc.nasa.gov/pdfs/Landsat7_Handbook.pdf

Jensen, J.R., 2000. Remote Sensing of the Environment: An Earth Resource Perspective. Prentice Hall, Upper Saddle River, NJ.

Li, J., Song, C., Cao, L., Zhu, F., Meng, X., Wu, J., 2011. Impacts of landscape structure on surface urban heat islands: a case study of Shanghai, China. Remote Sensing of Environment 115, 3249–3263.

Li, Y., Gong, P., Sasagawa, T., 2005. Integrated shadow removal based on photogrammetry and image analysis. International Journal of Remote Sensing 26 (18), 3911–3929.

Lo, C.P., Quattrochi, D.A., Luvall, J.C., 1997. Application of high-resolution thermal infrared remote sensing and GIS to assess the urban heat island effect. International Journal of Remote Sensing 18, 287–304.

Lu, D., 2007. Detection and substitution of clouds/hazes and their cast shadows on IKONOS images. International Journal of Remote Sensing 28, 4027–4035.

Lu, D., Hetrick, S., Moran, E., 2011. Impervious surface mapping with QuickBird imagery. International Journal of Remote Sensing 32 (9), 2519–2533.

Lu, D., Hetrick, S., Moran, E., Li, G., 2010. Detection of urban expansion in an urban–rural landscape with multitemporal QuickBird images. Journal of Applied Remote Sensing 4, 041880, http://dx.doi.org/10.1117/1.3501124.

Lu, D., Weng, Q., 2004. Spectral mixture analysis of the urban landscapes in Indianapolis with Landsat ETM+ imagery. Photogrammetric Engineering and Remote Sensing 70, 1053–1062.

Lu, D., Weng, Q., 2006. Spectral mixture analysis of ASTER imagery for examining the relationship between thermal features and biophysical descriptors in Indianapolis, Indiana. Remote Sensing of Environment 104 (2), 157–167.

Markham, B.L., Barker, J.L., 1986. Landsat MSS and TM post-calibration dynamic ranges, exoatmospheric reflectances and at-satellite temperatures. EOSAT Landsat Technical Notes, No. 1.

McCabe, M.F., Balick, L.K., Theiler, J., Gillespie, A.R., Mushkin, A., 2008. Linear mixing in thermal infrared temperature retrieval. International Journal of Remote Sensing 29, 5047–5061.

National Research Council, 2007. Earth Science and Applications from Space: National Imperatives for the Next Decade and Beyond. The National Academies Press, Washington, DC.

Nichol, J.E., 1994. A GIS based approach to microclimate monitoring in Singapore's high rise housing estates. Photogrammetric Engineering and Remote Sensing 60 (10), 1225–1232.
Nichol, J.E., 2005. Remote sensing of urban heat islands by day and night. Photogrammetric Engineering and Remote Sensing 71 (5), 613–621.
Okwen, R.T., Pu, R., Cunningham, J.A., 2011. Remote sensing of temperature variations around major power plants as point sources of heat. International Journal of Remote Sensing 32, 3791–3805.
Powell, R., Roberts, D.A., Hess, L., Dennison, P., 2007. Sub-pixel mapping of urban land cover using multiple endmember spectral mixture analysis: Manaus, Brazil. Remote Sensing of Environment 106 (2), 253–267.
Qin, Z., Karnieli, A., Berliner, P., 2001. Thermal variation in the Israel-Sinai (Egypt) peninsula region. International Journal of Remote Sensing 22 (6), 915–919.
Quattrochi, D.A., Luvall, J.C., 1999. Thermal infrared remote sensing for analysis of landscape ecological processes: methods and applications. Landscape Ecology 14, 577–598.
Quattrochi, D.A., Luvall, J.C., Estes Jr., M.G., Lo, C.P., Kidder, S.Q., Hafner, J., Taha, H., Bornstein, R.D., Gilles, R., Gallo, K.P., 1998. Project ATLANTA (Atlanta Land use Analysis: Temperature and Air quality): a study of how the urban landscape affects meteorology and air quality through time. In: Preprints, Second Urban Environment Symposium, 02–06 November, Albuquerque, New Mexico. American Meterological Society, Boston, Massachussetts, pp. 104–107.
Quattrochi, D.A., Luvall, J.C., Rickman, D.L., Estes Jr., M.G., Laymon, C.A., Howell, B.F., 2000. A decision support information system for urban landscape management using thermal infrared data. Photogrammetric Engineering and Remote Sensing 66 (10), 1195–1207.
Quattrochi, D.A., Ridd, M.K., 1994. Measurement and analysis of thermal energy responses from discrete urban surfaces using remote sensing data. International Journal of Remote Sensing 15 (10), 1991–2022.
Quattrochi, D.A., Ridd, M.K., 1998. Analysis of vegetation within a semiarid urban environment using high spatial resolution airborne thermal infrared remote sensing data. Atmospheric Environment 32 (1), 19–33.
Ridd, M., 1995. Exploring a V–I–S (vegetation–impervious–surface-soil) model for urban ecosystem analysis through remote sensing: comparative anatomy for cities. International Journal of Remote Sensing 16, 2165–2185.
Roberts, D.A., Gardner, M., Church, R., Ustin, S., Scheer, G., Green, R.O., 1998. Mapping chaparral in the Santa Monica Mountains using multiple endmember spectral mixture models. Remote Sensing of Environment 65, 267–279.
Roberts, D.A., Quattrochi, D.A., Hulley, G.C., Hook, S.J., Green, R.O., 2012. Synergies between VSWIR and TIR data for the urban environment: an evaluation of the potential for the Hyperspectral Infrared Imager (HyspIRI) Decadal Survey mission. Remote Sensing of Environment 117, 83–101.
Rocken, C., Van Hove, T., Johnson, J., Solheim, F., Ware, R., Bevis, M., Businger, S., Chiswell, S., 1995. GPS/Storm–GPS sensing of atmospheric water vapor for meteorology. Journal of Atmospheric and Oceanic Technology 12, 468–478.
Shoshany, M., Aminov, R., Goldreich, Y., 1994. The extraction of roof tops from thermal imagery for analyzing the urban heat island structure. Geocarto International 4, 61–69.
Somers, B., Delalieux, S., Stuckens, J., Verstraeten, W.W., Coppin, P., 2009. A weighted Linear Spectral Mixture Analysis approach to address endmember variability in agricultural production systems. International Journal of Remote Sensing 30, 139–147.
Small, C., 2001. Estimation of urban vegetation abundance by spectral mixture analysis. International Journal of Remote Sensing 22, 1305–1334.
Smith, M.O., Ustin, S.L., Adams, J.B., Gillespie, A.R., 1990. Vegetation in Deserts. I. A regional measure of abundance from multispectral images. Remote Sensing of Environment 31, 1–26.
Sobrino, J.A., Raissouni, N., Li, Z.-L., 2001. A comparative study of land surface emissivity retrieval from NOAA data. Remote Sensing of Environment 75, 256–266.
Southeastern Wisconsin Regional Planning Commission, 2000. Land Use Classifications and Codes: SEWRPC Regional Land Use Inventory 2000.
Southeastern Wisconsin Regional Planning Commission, 2004a. The population of Southeastern Wisconsin, technical report #11 (4th ed.). Available online at: http://www.sewrpc.org/SEWRPCFiles/publications/techrep/tr-011_population_southeastern_wisconsin.pdf (assessed 26.05.12).
Southeastern Wisconsin Regional Planning Commission, 2004b. The Economy of Southeastern Wisconsin, technical report #10 (4th ed.). Available online at: http://www.sewrpc.org/SEWRPCFiles/Publications/TechRep/tr-010_economy_southeastern_wisconsin.pdf (assessed 26.05.12).
Streutker, D.R., 2002. A remote sensing study of the urban heat island of Houston, Texas. International Journal of Remote Sensing 23, 2595–2608.
Streutker, D.R., 2003. Satellite-measured growth of the urban heat island of Houston, Texas. Remote Sensing of Environment 85 (3), 282–289.
Taylor, M., 2009. IKONOS planetary reflectance and mean solar exoatmospheric irradiance. GeoEye Technical paper.
U.S. Geological Survey, 2010. Landsat Update: New Thermal Band Resampling: 30-meter pixels. Available online at: http://landsat.usgs.gov/documents/about_LU_Vol_4_Issue_Special_Edition.pdf
Van der Meer, F., De Jong, S.M., 2000. Improving the results of spectral unmixing of Landsat Thematic Mapper imagery by enhancing the orthogonality of endmembers. International Journal of Remote Sensing 21, 2781–2797.
Van der Meer, F.D., Jia, X.P., 2012. Collinearity and orthogonality of endmembers in linear spectral unmixing. International Journal of Applied Earth Observation and Geoinformation 18, 491–503.
Voogt, J.A., Oke, T.R., 2003. Thermal remote sensing of urban areas. Remote Sensing of Environment 86, 370–384.
Weng, Q., 2009. Thermal infrared remote sensing for urban climate and environmental studies: methods, applications, and trends. ISPRS Journal of Photogrammetry and Remote Sensing 64 (4), 335–344.
Weng, Q., Liu, H., Liang, B., Lu, D., 2008. The spatial variations of urban land surface temperatures: pertinent factors, zoning effect, and seasonal variability. IEEE Journal Selected Topics in Applied Earth Observations and Remote Sensing 1 (2), 154–166.
Weng, Q., Rajasekar, U., Hu, X., 2011. Modeling urban heat islands and their relationship with impervious surface and vegetation abundance by using ASTER images. IEEE Transactions on Geoscience and Remote Sensing 49, 4080–4089.
Wu, C., Murray, A.T., 2003. Estimating impervious surface distribution by spectral mixture analysis. Remote Sensing of Environment 84, 493–505.
Wu, C., 2004. Normalized spectral mixture analysis for monitoring urban composition using ETM+ imagery. Remote Sensing of Environment 93, 480–492.
Wu, C., 2009. Quantifying high-resolution impervious surfaces using spectral mixture analysis. International Journal of Remote Sensing 30 (11), 2915–2932.
Yuan, F., Bauer, M.E., 2007. Comparison of impervious surface area and normalized difference vegetation index as indicators of surface urban heat island effects in Landsat imagery. Remote Sensing of Environment 106, 375–386.